Cell culture and growth-arrest assays. Human foreskin keratinocytes, fibroblasts and mammary epithelial cells were isolated as described[9,13]. HFKs were grown in keratinocyte serum-free medium (K-SFM; Gibco-BRL), HMEC were grown in DFCI-1 (ref. 13) and HFFs were grown in 10% FBS DMEM (Gibco-BRL). Epithelial cells and fibroblasts were selected in 50–100 $\mu g\,ml^{-1}$ and 1,000 $\mu g\,ml^{-1}$ G418, respectively, or 40 $\mu g\,ml^{-1}$ hygromycin B after retroviral infection. HFK and HMEC were infected by PD 4–10, whereas HFF were infected at PD 30. Clones were isolated by cylinder isolation of colonies. HFKs were split 1:4 at early passages, and 1:8 thereafter using trypsin/EDTA. HMEC were fed every other day and passaged at a ratio of 1:5 or 1:10 before cultures were confluent. Fibroblasts were split 1:16. Cells in crisis or senescence were fed 3 to 4 times weekly, split if necessary, and maintained until there was no visible sign of proliferation (usually 2 months). Subconfluent cultures of retrovirally infected HMEC expressing various E6 genes were treated with 2.5 nM actinomycin D and growth arrest assayed as described[21].

TRAP and telomerase length assays. The telomere repeat amplification protocol (TRAP) assay was performed with several modifications to the original protocol[28] in order to control for false positives and inhibitors of PCR amplification. Cells were counted and lysed in CHAPS lysis buffer at a concentration of 6,400 cells per μl buffer and 1 μl was used for the TRAP assay. This number of cells was within the range of exponential amplification of products in the TRAP assay using positive control cells that had high telomerase activity. The TS primer was kinase-labelled with [γ-^{32}P]ATP and used at 25×10^6 c.p.m. μg^{-1}. The CX-ext primer is a modification of the original CX primer and was designed to prevent primer–dimer interactions and false positives[29]. An internal ITAS fragment was included to control for the PCR reaction[30]. PCR cycles were carried out as described and one-eighth of the sample was run on a 7.2% non-denaturing polyacrylamide gel. Relative telomerase signal intensity of the repeat bands was measured by phosphor imaging analysis. Telomere length was assayed as described[18].

Western and northern blot analyses. 20 μg protein from whole-cell extracts was separated by SDS–PAGE and blots were prepared on Immobilon-P membrane (Millipore). The following antibodies were used as probes: for p53 and p21, clones DO-1 and EA-10 (Oncogene Science); for Rb and p16, clones G3-245 and G175-405 (PharMingen); and for p27, K25020 (Transduction Laboratories). Blots were then probed with horseradish-peroxidase-conjugated goat anti-mouse IgG (Jackson ImmunoResearch) and visualized by using the chemiluminescence system (Renaissance; Du Pont NEN). For northern blots, 16 μg total RNA per lane was separated on formaldehyde–agarose gels, transferred to Hybond N membranes (Amersham) and probed with a p16-exon 1β probe, specific for ARF. Blots were reprobed for acidic ribosomal protein-PO (36B4) as a loading control.

Received 15 May; accepted 27 August 1998.

1. Hayflick, L. The limited *in vitro* lifespan of human diploid cell strains. *Exp. Cell Res.* **37,** 614–621 (1965).
2. Loughran, O. *et al.* Evidence for the inactivation of multiple replicative lifespan genes in immortal human squamous cell carcinoma keratinocytes. *Oncogene* **14,** 1955–1964 (1997).
3. Alcorta, D. A. *et al.* Involvement of the cyclin-dependent kinase inhibitor p16 (INK4a) in replicative senescence of normal human fibroblasts. *Proc. Natl Acad. Sci. USA* **93,** 13742–13747 (1996).
4. Allsopp, R. C. *et al.* Telomere length predicts replicative capacity of human fibroblasts. *Proc. Natl Acad. Sci. USA* **89,** 10114–10118 (1992).
5. Bodnar, A. G. *et al.* Extension of life-span by introduction of telomerase into normal human cells. *Science* **279,** 349–352 (1998).
6. Wright, W. E. & Shay, J. W. The two-stage mechanism controlling cellular senescence and immortalization. *Exp. Gerontol.* **27,** 383–389 (1992).
7. Hawley-Nelson, P., Vousden, K. H., Hubbert, N. L., Lowy, D. R. & Schiller, J. T. HPV 16 E6 and E7 proteins cooperate to immortalize human foreskin keratinocytes. *EMBO J.* **8,** 3905–3910 (1989).
8. Munger, K., Phelps, W. C., Bubb, V., Howley, P. M. & Schlegel, R. The E6 and E7 genes of the human papillomavirus type 16 together are necessary and sufficient for transformation of primary human keratinocytes. *J. Virol.* **63,** 4417–4421 (1989).
9. Halbert, C. L., Demers, G. W. & Galloway, D. A. The E7 gene of human papillomavirus type 16 is sufficient for immortalization of human epithelial cells. *J. Virol.* **65,** 474–478 (1991).
10. Foster, S. A. & Galloway, D. A. Human papillomavirus type 16 E7 alleviates a proliferation block in early passage human mammary epithelial cells. *Oncogene* **12,** 1773–1779 (1996).
11. Foster, S. A., Wong, D. J., Barrett, M. T. & Galloway, D. A. Inactivation of p16 in human mammary epithelial cells by CpG island methylation. *Mol. Cell. Biol.* **18,** 1793–1801 (1998).
12. Shay, J. W., Wright, W. E., Brasiskyte, D. & van der Haegen, B. A. E6 of human papillomavirus type 16 can overcome the M1 stage of immortalization in human mammary epithelial cells but not in human fibroblasts. *Oncogene* **8,** 1407–1413 (1993).
13. Band, V., Zajchowski, D., Kulesa, V. & Sager, R. Human papilloma virus DNAs immortalize normal human mammary epithelial cells and reduce their growth factor requirements. *Proc. Natl Acad. Sci. USA* **87,** 463–467 (1990).
14. Shay, J. W., van der Haegen, B. A., Ying, Y. & Wright, W. E. The frequency of immortalization of human fibroblasts and mammary epithelial cells transfected with SV40 large T-antigen. *Exp. Cell Res.* **209,** 45–52 (1993).
15. Nakamura, T. M. *et al.* Telomerase catalytic subunit homologs from fission yeast and human. *Science* **277,** 955–959 (1997).
16. Klingelhutz, A. J., Foster, S. A. & McDougall, J. K. Telomerase activation by the E6 gene product of human papillomavirus type 16. *Nature* **380,** 79–82 (1996).
17. Wang, J., Xie, L. Y., Allan, S., Beach, D. & Hannon, G. J. Myc activates telomerase. *Genes Dev.* **12,** 1769–1774 (1998).
18. Klingelhutz, A. J., Barber, S. A., Smith, P. P., Dyer, K. & McDougall, J. K. Restoration of telomeres in human papillomavirus-immortalized human anogenital epithelial cells. *Mol. Cell. Biol.* **14,** 961–969 (1994).
19. Stoppler, H., Hartmann, D. P., Sherman, L. & Schlegel, R. The human papillomavirus type 16 E6 and E7 oncoproteins dissociate cellular telomerase activity from the maintenance of telomere length. *J. Biol. Chem.* **272,** 13332–13337 (1997).
20. Khleif, S. N. *et al.* Inhibition of cyclin D-CDK4/CDK6 activity is associated with an E2F mediated induction of cyclin kinase inhibitor activity. *Proc. Natl Acad. Sci. USA* **93,** 4350–4354 (1996).
21. Demers, G. W., Foster, S. A., Halbert, C. L. & Galloway, D. A. Growth arrest by induction of p53 in DNA damaged keratinocytes is bypassed by human papillomavirus 16 E7. *Proc. Natl Acad. Sci. USA* **91,** 4382–4386 (1994).
22. Scheffner, M., Werness, B. A., Huibregtse, J. M., Levine, A. J. & Howley, P. M. The E6 oncoprotein encoded by human papillomavirus types 16 and 18 promotes the degradation of p53. *Cell* **63,** 1129–1136 (1990).
23. Kiyono, T. *et al.* Binding of high risk human papillomavirus E6 oncoproteins to the human homologue of the *Drosophila* discs large tumor suppressor protein. *Proc. Natl Acad. Sci. USA* **94,** 11612–11616 (1997).
24. Dalal, S., Gao, Q., Androphy, E. J. & Band, V. Mutational analysis of human papillomavirus type 16 E6 demonstrates that p53 degradation is necessary for immortalization of mammary epithelial cells. *J. Virol.* **70,** 683–688 (1996).
25. Kamijo, T. *et al.* Tumor suppression at the mouse INK4A locus mediated by the alternative reading frame product p19ARF. *Cell* **91,** 649–659 (1997).
26. Gross-Mesilaty, S. *et al.* Basal and human papillomavirus E6 oncoprotein-induced degradation of Myc proteins by the ubiquitin pathway. *Proc. Natl Acad. Sci. USA* **95,** 8058–8063 (1998).
27. Huibregtse, J. M., Scheffner, M. & Howley, P. M. Cloning and expression of the cDNA for E6-AP, a protein that mediates the interaction of the human papillomavirus E6 oncoprotein with p53. *Mol. Cell. Biol.* **13,** 775–784 (1993).
28. Kim, N. W. *et al.* Specific association of human telomerase activity with immortal cells and cancer. *Science* **266,** 2011–2015 (1994).
29. Krupp, G. *et al.* Molecular basis of artifacts in the detection of telomerase activity and a modified primer for a more robust 'TRAP' assay. *Nucleic Acids Res.* **25,** 919–921 (1997).
30. Wright, W. E., Shay, J. W. & Piatyszek, M. A. Modifications of a telomeric repeat amplification protocol (TRAP) result in increased reliability, linearity and sensitivity. *Nucleic Acids Res.* **23,** 3794–3795 (1995).

Acknowledgements. We thank the Geron Corporation for the hTERT cDNA, E. Espling for maintaining stocks of retroviruses, the Image Analysis Laboratory for help with preparing figures, and members of the McDougall and Galloway laboratories for discussion. This work was supported by grants from the NIH to J.K.M. and D.A.G.

Correspondence and requests for materials should be addressed to D.A.G. (e-mail: dgallowa@fhcrc.org).

NMR structure of the histidine kinase domain of the *E. coli* osmosensor EnvZ

Toshiyuki Tanaka*, Soumitra K. Saha†, Chieri Tomomori*, Rieko Ishima‡, Dingjiang Liu‡, Kit I. Tong‡, Heiyoung Park†, Rinku Dutta†, Ling Qin†, Mark B. Swindells§‖, Toshimasa Yamazaki¶, Akira M. Ono#, Masatsune Kainosho#, Masayori Inouye† & Mitsuhiko Ikura‡

** Center for Tsukuba Advanced Research Alliance and Institute of Applied Biochemistry, University of Tsukuba, Tsukuba 305-8577, Japan*
† Department of Biochemistry, Robert Wood Johnson Medical School, University of Medicine and Dentistry of New Jersey, New Jersey 08854, USA
‡ Division of Molecular and Structural Biology, Ontario Cancer Institute and Department of Medical Biophysics, University of Toronto, 610 University Avenue, Toronto, Ontario M5G 2M9, Canada
§ Helix Research Institute Inc., Kisarazu 292-0812, Japan
¶ National Institute of Agrobiological Resources, Tsukuba 305-0856, Japan
 # Department of Chemistry, Tokyo Metropolitan University, Hachioji 192-0397, Japan

Bacteria live in capricious environments, in which they must continuously sense external conditions in order to adjust their shape, motility and physiology[1]. The histidine–aspartate phosphorelay signal-transduction system (also known as the two-component system) is important in cellular adaptation to environmental changes in both prokaryotes and lower eukaryotes[2,3]. In

‖ Present address: Inpharmatica Ltd, 60 Charlotte Street, London W1P 2AX, UK

this system, protein histidine kinases function as sensors and signal transducers. The *Escherichia coli* osmosensor, EnvZ, is a transmembrane protein with histidine kinase activity in its cytoplasmic region[2]. The cytoplasmic region contains two functional domains[4]: domain A (residues 223–289) contains the conserved histidine residue (H243), a site of autophosphorylation as well as transphosphorylation to the conserved D55 residue of response regulator OmpR, whereas domain B (residues 290–450) encloses several highly conserved regions (G1, G2, F and N boxes) and is able to phosphorylate H243. Here we present the solution structure of domain B, the catalytic core of EnvZ. This core has a novel protein kinase structure, distinct from the serine/threonine/tyrosine kinase fold, with unanticipated similarities to both heat-shock protein 90 and DNA gyrase B.

The catalytic domain of EnvZ (Fig. 1a, b) assumes an α/β-sandwich fold: one layer consists of a five-stranded β-sheet (strands B, residues 319–323; D, 356–362; E, 367–373; F, 420–423; and G, 431–436), and the other layer comprises three α-helices (α1, residues 301–311; α2, 334–343; and α4, 410–414). Two adjacent parallel β-strands, B and D, which are connected by helix α2, exhibit an unusual 'left-handed' connectivity[5] (see below). The two layers enclose an extensive hydrophobic core, augmented by a small antiparallel β-sheet (strands A, residues 297–299; and C, 330–332) that seals the sandwich at one end. A number of structurally vital hydrophobic residues (Fig. 1c) are highly conserved in homologous histidine kinase domains, as would be expected. A striking feature in the EnvZ fold is the presence of a long polypeptide segment that extends away from the rest of the molecule (Fig. 1b). This segment consists of a short α-helix, α3 (residues 380–384), followed by a long loop (residues 385–409), which we refer to as the

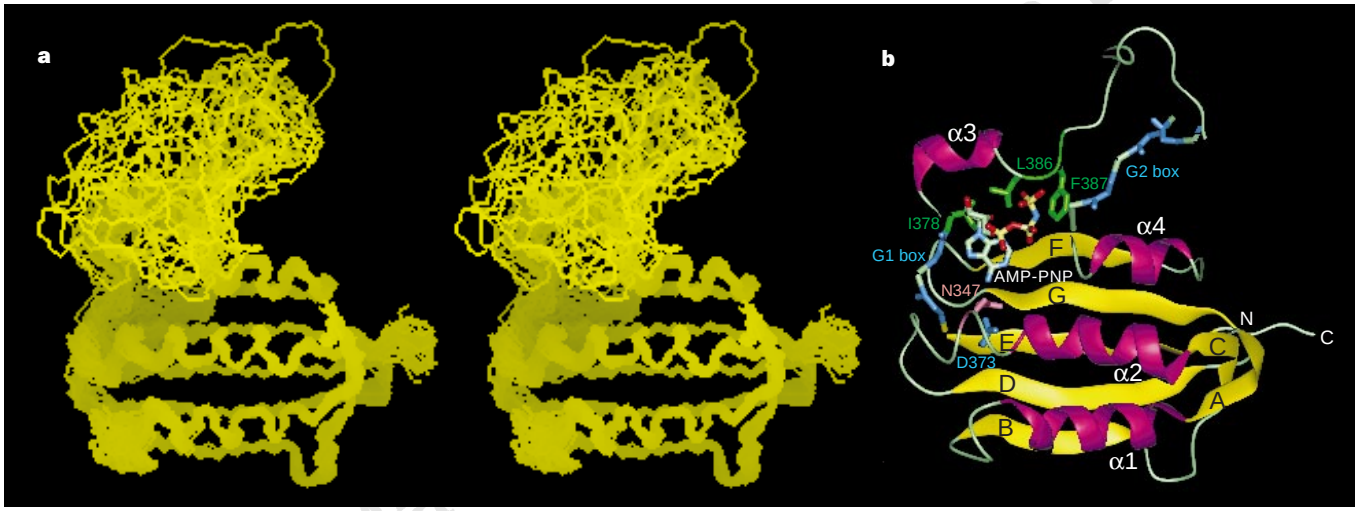

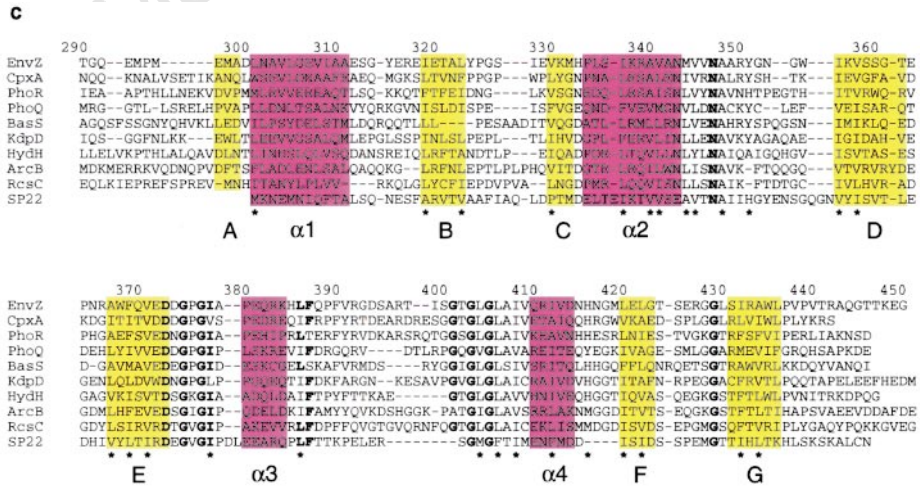

Figure 1 Sequence and structure of the EnvZ catalytic domain. **a**, Stereoview of a best-fit superposition of the backbone (N, Cα and C′) atoms of the 25 NMR-derived structures of the EnvZ catalytic domain, generated using Insight II (Molecular Simulations). The main-chain atoms of the 25 structures are superimposed against the energy-minimized average structure using residues 297–299, 301–311, 319–323, 330–332, 334–343, 356–362, 367–373, 420–423 and 431–436 (r.m.s.d. of 0.57 ± 0.12 Å for backbone atoms and 0.94 ± 0.08 Å for all heavy atoms). The central loop region is less well-defined because of its flexibility. The N-terminal five and C-terminal ten residues, which are also not well-defined because of the lack of many experimental distance and dihedral angle restraints, are omitted in the figure. **b**, Ribbon drawing of the energy-minimized average structure of the EnvZ catalytic domain. The ATP analogue (AMP-PNP) is shown as a stick model, and the α-helices (in magenta) and β-strands (in yellow) are labelled. The backbone heavy atoms of the glycines in the G1 and G2 boxes (in blue), and the sidechain heavy atoms of N347 (in pink), D373 (in blue), and I378, L386 and F387 (in green) are also shown as stick models. The N-terminal five and C-terminal ten residues are omitted as in **a**. The N and C termini of the protein are also indicated. The model was generated using QUANTA (Molecular Simulations). **c**, Sequence alignment of the EnvZ catalytic domain with other members of the histidine kinase family. The accession numbers of the SWISS-PROT database for the sequences are P02933 (EnvZ), P08336 (CpxA), P08400 (PhoR), P23837 (PhoQ), P30844 (BasS), P21865 (KdpD), P14377 (HydH), P22763 (ArcB), P14376 (RcsC), and P10728 (SpoIIAB; labelled as SP22 in the figure). Secondary structural elements are shown by boxes coloured as in **b**, with their notation indicated below the boxes. Asterisks denote the conserved hydrophobic amino-acid residues. The residues that are important in the ATP binding are shown in bold.

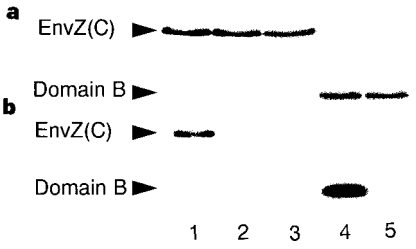

Figure 2 Identification of the ATP-binding domain in EnvZ and the involvement of N347 in ATP binding. **a**, **b**, Ultraviolet-crosslinked protein (see Methods) was visualized through autoradiography (**b**) after 17.5% SDS–PAGE. An identical amount of each protein was used as shown by the CMB-stained SDS–PAGE (**a**). The crosslinked proteins are as follows: lane 1, EnvZ(223–450) (labelled as EnvZ(C) in the figure) with 10 μCi [α-^{32}P]ATP; lane 2, EnvZ(223–450) with 10 μCi [α-^{32}P]ATP and 500 μM non-radioactive ATP; lane 3, EnvZ-N347D(223–450) with 10 μCi [α-^{32}P]ATP; lane 4, EnvZ(290–450) (labelled as domain B in the figure) with 50 μCi [γ-^{32}P]ATP; lane 5, EnvZ(290–450) with 50 μCi [γ-^{32}P]ATP and 1 mM non-radioactive ATP.

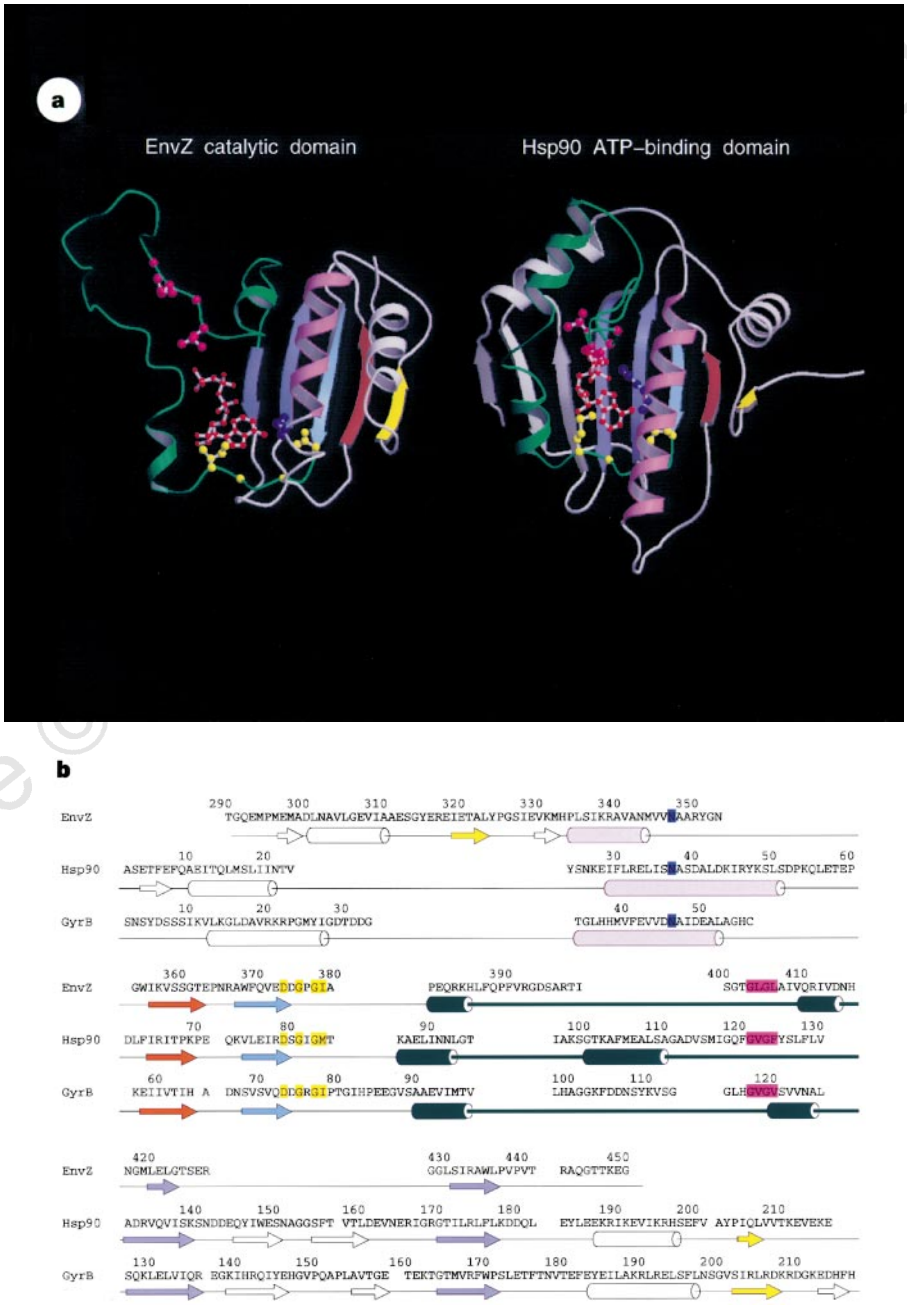

Figure 3 EnvZ and Hsp90 have a similar fold in their ATP-binding regions. **a**, Ribbon representation of the EnvZ catalytic domain and the ATP-binding domain of the molecular chaperone Hsp90 (Protein DataBank accession number 1amw)[9]. For the EnvZ catalytic domain, strand B is shown in yellow, strand D in orange, strand E in light blue, strands F and G in purple, helix α2 in pink, and the central loop including helices α3 and α4 in green. Heavy atoms (except N, C and O) of N347 (in blue), D373, G375, G377 and I378 (in yellow), and G403, L404, G405 and L406 (in magenta) are shown as ball-and-stick models. The corresponding secondary structural elements and specific residues of Hsp90 are coloured as for EnvZ. AMP-PNP (ADP in Hsp90) is also shown as a ball-and-stick model, in red. The model was generated using MOLSCRIPT[20] and Raster3D[21]. **b**, Alignment of the amino-acid sequences of the EnvZ catalytic domain and the ATP-binding domains of Hsp90 and DNA gyrase B (GyrB)[9,22], found by the SSAP program[23]. α-Helices and β-strands of each structure are indicated as cylinders and arrows, respectively. The colour coding for the secondary structure elements and highlighted residues is as in **a**.

central loop. We detected almost no medium- or long-range nuclear Overhauser effects (NOEs) for the residues in this loop, and the chemical shifts and backbone coupling constants ($^3J_{NH\alpha}$) were nearly the same as those in a random coil (data not shown). Moreover, $^1H-^{15}N$ heteronuclear NOE measurements showed smaller NOE values (0.49 ± 0.10) for the residues in this loop than the values (0.75 ± 0.12) for the structurally well-defined region, further indicating that the region is mobile in solution. The lack of domain A in our NMR structure may be responsible for the high mobility of this central loop. The loop is near to the nucleotide-binding site (see below) and probably interacts with the H243 phosphorylation site and/or its neighbouring residues in domain A.

Like eukaryotic protein kinases, histidine kinases require the presence of ATP and Mg^{2+} for their activity[6]. Non-radioactive ATP competes with [α-^{32}P]ATP for binding to the whole cytoplasmic domain of EnvZ (residues 223–450) (Fig. 2, lanes 1, 2). This ATP-binding function is retained in domain B (Fig. 2, lane 4); non-radioactive ATP competes with [γ-^{32}P]ATP for binding to this domain (Fig. 2, lane 5). Our domain B structure contains a non-hydrolysable analogue of ATP, AMP-PNP (β,γ-imidoadenosine-5′-triphosphate), whose location in the structure has been determined on the basis of a dozen intermolecular NOEs observed between sidechain protons of I378/L386/L422 and the adenosine H2, H8, H1′, H4′ and H5′ protons. The AMP-PNP molecule is surrounded by helix α3 and part of the central loop, and makes extra contacts with strands F and G. The AMP-PNP adenine ring is in close spatial proximity to N347, D373, I378, L386 and F387 (Fig. 1b), which are conserved in members of the histidine kinase family (Fig. 1c). The triphosphate chain is exposed to the protein surface, consistent with the potential for transferring the γ-phosphate to H243 in domain A. In addition, five glycines (G375, G377, G403, G405 and G429) and an asparagine (N347) in the catalytic core are highly conserved and strategically located in the structure (Fig. 1b), indicating their structural and functional significance. Previous mutagenesis studies[7] showed that the glycine-rich regions, G1 (D373–G377) and G2 (G403–G405), are essential for kinase activity. In addition our structure shows that G375 and G429 are particularly important, allowing sharp kinks (between strand E and helix α3 and between strands F and G, respectively) that contour part of the AMP-PNP-binding site.

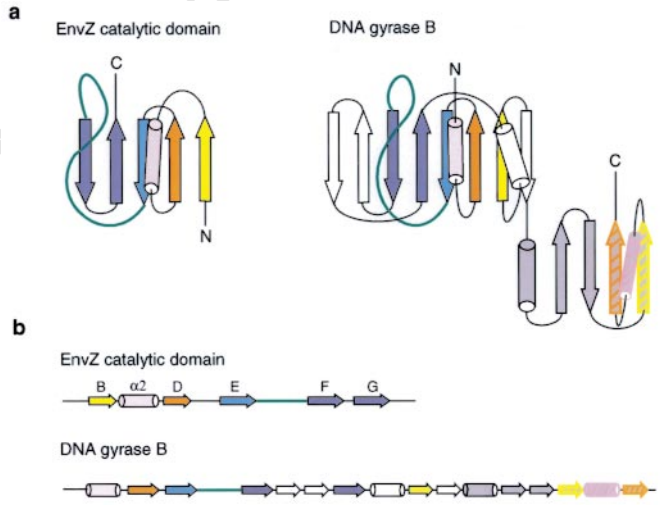

Figure 4 The EnvZ catalytic domain and DNA gyrase B. **a**, Secondary structure; **b**, the linear arrangement of structural elements. This figure emphasizes the recurrence of aligned structural elements involved in the ATP-binding sites (coloured) and the position of the left-handed $\beta\alpha\beta$ motif in each structure (EnvZ, yellow–pink–orange; DNA gyrase B, hashed regions of the same colours). α-Helices and β-strands of each structure are indicated as cylinders and arrows, respectively. The colour coding for the secondary structure elements is the same as in Fig. 3a except for the C-terminal domain of the DNA gyrase B subunit. The N and C termini of each structure are indicated.

High deviation of the central loop in the NMR-derived structure, due to high mobility, precludes close examination of the residues that could be involved in the catalysis. However, further information can be obtained from several data base searches and structural comparisons. While the structure of EnvZ domain B was being determined, we noted that detailed Ψ-BLAST searches[8] indicated a distant similarity of domain B with both heat-shock protein 90 (Hsp90) (ref. 9) and DNA gyrase B[10]. Although the Ψ-BLAST scores were low, this potential relationship was particularly interesting, because first, all these proteins must bind ATP to fulfil their functions, and second, the ATP-binding domains of Hsp90 and DNA gyrase B were already known to have similar folds[9]. Upon determination, close examination of these structures indicated that the EnvZ fold is indeed similar to the fold found in the ATP-binding regions of Hsp90 and the DNA gyrase B (Fig. 3). Common to all three families are helix α2, four strands (D, E, F and G) and the central loop (residues 385–409). Together they enclose N347, the G1 (DxGxGϕ) motif (residues 373–378), and the G2 (GϕGϕ) motif (residues 403–406) (x represents any amino acid; ϕ represents a hydrophobic amino acid), which occur in all three families and are close to the ATP-binding site of Hsp90 (Protein DataBank codes 1amw and 1am1).

In detail, residue N37 of the Hsp90-ADP complex (corresponding to N347 in EnvZ) binds directly to β-phosphate and Mg^{2+} and indirectly to the adenine base[9]. Expression of an EnvZ mutant protein in which N347 is mutated to aspartate (N347D) results in a phenotype in which ATP-dependent autokinase activity is lost; however, the ability of the mutant protein to phosphorylate OmpR is retained[11]. The importance of N347 is shown in Fig. 2 (lane 3): ATP binding to EnvZ residues 223–450 is abolished in the N347D mutant. Decreased affinity of the N347D mutant for ATP is evidence that this conserved asparagine is vital for the ATP-dependent autophosphorylation activity of EnvZ. In the structures of both Hsp90 and DNA gyrase, the only highly conserved charged residue, aspartate in the DxGxGϕ motif (D79 and D73 in Hsp90 and DNA gyrase, respectively), interacts with the N6 atom in the adenine base[9,10]. The corresponding residue in EnvZ, D373, is also close to the N6 atom of AMP-PNP in our structure (Fig. 1b).

Despite the clear similarity between EnvZ, Hsp90 and DNA gyrase B, EnvZ initially appears to be the outlier of the trio, mainly because of the left-handed $\beta\alpha\beta$ connection between strands B and D. Cases of clear left-handed connectivity are quite rare despite the present availability of more than 1,000 non-homologous structures. It is, therefore, all the more surprising that one such case is found in the carboxy-terminal, DNA-binding domain of *E. coli* DNA gyrase B (Fig. 4). The similarity of the ATP-binding domain, coupled with the presence of a left-handed $\beta\alpha\beta$ connection in both proteins, supports the possibility of a distant evolutionary link between these two protein families.

In an analysis of 11 completed genomes using the EnvZ catalytic domain we identified nearly 150 homologous sequences, using Ψ-BLAST search[8] with an expectation (E) value of 0.01. In a similar search of the non-redundant OWL database we identified over 400 such sequences. These included proteins such as anti-sigma factor[12] (SpoIIAB). On the *E. coli* chromosome, genes encoding 32 histidine kinases have been identified[13], and 17 of these kinases have been characterized biochemically[2]. The sequence of Sln1, an osmosensor in yeast[14], is conserved in all regions corresponding to secondary structural elements in EnvZ, but contains a 120-residue insertion between strands D and E of the EnvZ structure. This indicates that the yeast histidine kinase contains the same fold as that of EnvZ, with a modification between the two strands, presumably resulting in additional functionality.

There are at least 100 examples of histidine–aspartate phosphorelays

in bacteria, and some are implicated in bacterial virulence[2]. For example, a life-threatening bacterium, *Salmonella typhimurium*, possesses the PhoP/PhoQ phosphorelay system which seems to be essential for its virulence in host organisms[15]. As all of these phosphorelay systems contain a conserved histidine kinase domain, which has not been found in mammalian cells, histidine kinases are excellent targets for antimicrobial action[16]. Members of a family of hydrophobic tyramines have already been identified as histidine kinase inhibitors; the half-maximal inhibitory concentration of these inhibitors is 2–600 μM (ref. 17). Our structure of the *E. coli* EnvZ histidine kinase catalytic domain will provide a vital foundation for the rational design of potent antibiotics that specifically inhibit multiple histidine kinases in this and other microbial species. □

Methods

Sample preparation. Recombinant uniformly ^{15}N- and ^{13}C-labelled EnvZ was expressed in overproducing *E. coli* strain pET11a/BL21(DE3) grown in M9 minimal medium, and was purified as described[4]. NMR samples contained 1.0–1.5 mM uniformly ^{15}N- or ^{13}C/^{15}N-labelled, or unlabelled, protein in either 95% H_2O/5% ^2H_2O or 99.996% ^2H_2O containing 20 mM sodium phosphate, 50 mM KCl, 0.5 mM 4-(2-aminoethyl)-benzenesulphonyl fluoride, 50 μM sodium azide and 5 mM $MgCl_2$, pH 7.0, with 5 mM unlabelled or ^{15}N/^{13}C-labelled AMP-PNP.

NMR spectroscopy. All NMR spectra were acquired at 25 °C on Varian UNITY-plus 500, UNITY-600, and Bruker DMX750 spectrometers. ^{1}H, ^{13}C, and ^{15}N resonances of the backbone were assigned by analysing four triple-resonance experiments, (HB)CBCA(CO)NNH, HNCACB, (HB)CBCACO(CA)HA, and HNCO. Assignment of the sidechain resonances was done using the three-dimensional HCCH-TOCSY and ^{13}C-edited NOESY-HMQC spectra. $^3J_{NH\alpha}$ coupling constants were measured from ^{1}H/^{15}N HMQC-J spectrum, and slow-exchanging amide proteins were identified by recording a series of gradient-enhanced ^{1}H-^{15}N HSQC spectra at different time points immediately after the H_2O buffer was changed to a ^2H_2O buffer.

Structure calculation. Structure calculations were done using a restrained molecular dynamics simulated annealing protocol[18] within X-PLOR[19]. For structure calculations we used 1,782 interproton distance restraints (comprising 556 intraresidue, 440 sequential, 260 short-range, 507 long-range, 13 protein–ATP analogue, and 10 intra-analogue distances) obtained from heteronuclear three-dimensional NOE spectra. In addition to the NOE-derived distance restraints, 92 distance restraints for 46 hydrogen bonds and 122 dihedral angle restraints were included in the structure calculation. The average root mean square deviation (r.m.s.d.) values from idealized geometry for bonds, angles and impropers are 0.005 Å, 0.61° and 0.39°, respectively. The total and Lennard–Jones potential energies are 516 ± 70 and -134 ± 29 kcal mol^{-1}, respectively (calculated with the use of square-well potentials for the experimental distance empirical energy term with a force constant of 50 kcal mol^{-1} Å^{-2}). None of the structures has violations greater than 0.40 Å (for distance restraints) and 3.0° (for dihedral angle restraints).

Ultraviolet-crosslinking assay. Purified proteins were each incubated in crosslinking buffer (20 mM Tris, pH 7.8, 50 mM KCl and 5% glycerol) containing [α-^{32}P]ATP (800 Ci mmol^{-1}, 10 mCi ml^{-1}) or [γ-^{32}P]ATP (3,000 Ci mmol^{-1}, 10 mCi ml^{-1}) in a final volume of 25 μl for 15 min at 4 °C. Proteins were crosslinked by ultraviolet irradiation at 254 nm at a height of 4.5 cm for 5 min on ice using an ultraviolet lamp (Model UVG-45, 115 V, 60 Hz, 0.16 A, UVP Inc., California). Crosslinked protein was visualized by autoradiography after analysis by 17.5% SDS–PAGE. For competition experiments, non-radioactive ATP was added in the reaction mixture.

Received 19 June; accepted 12 August 1998.

1. Parkinson, J. S. in *Two-Component Signal Transduction* (eds Hock, J. A. & Silhavy, T. J.) 9–23 (ASM, Washington, DC, 1995).
2. Egger, L. A., Park, H. & Inouye, M. Signal transduction via the histidyl-aspartyl phosphorelay. *Genes Cells* **2,** 167–184 (1997).
3. Wirgler-Murphy, S. M. & Saito, H. Two-component signal transducers and MAPK cascades. *Trends Biochem. Sci.* **22,** 172–176 (1997).
4. Park, H., Saha, S. K. & Inouye, M. Two-domain reconstitution of a functional protein histidine kinase. *Proc. Natl Acad. Sci. USA* **95,** 6728–6732 (1998).
5. Branden, C. & Tooze, J. *Introduction to Protein Structure* (Garland, New York, 1991).
6. Stock, J. B., Surette, M. G., Levit, M. & Park, P. in *Two-Component Signal Transduction* (eds Hock, J. A. & Silhavy, T. J.) 25–51 (ASM, Washington, DC, 1995).
7. Yang, Y. & Inouye, M. Requirement of both kinase and phosphatase activities of an *Escherichia coli* receptor (Tazl) for ligand-dependent signal transduction. *J. Mol. Biol.* **231,** 335–342 (1993).
8. Altschul, S. F. *et al.* Gapped BLAST and PSI-BLAST: a new generation of protein database search programs. *Nucleic Acids Res.* **25,** 3389–3402 (1997).
9. Prodromou, C. *et al.* Identification and structural characterization of the ATP/ADP-binding site in the Hsp90 molecular chaperone. *Cell* **90,** 65–75 (1997).
10. Wigley, D. B. *et al.* Crystal structure of an N-terminal fragment of the DNA gyrase B protein. *Nature* **351,** 624–629 (1991).
11. Dutta, R. & Inouye, M. Reverse phosphotransfer from OmpR to EnvZ in a kinase$^-$/phosphatase$^+$ mutant of EnvZ (EnvZ·N347D), a bifunctional signal transducer of *Escherichia coli*. *J. Biol. Chem.* **271,** 1424–1429 (1996).
12. Min, K.-T. *et al.* Sigma F, the first compartment-specific transcription factor of *B. subtilis*, is regulated by anti-sigma factor that is also a protein kinase. *Cell* **27,** 735–742 (1993).
13. Mizuno, T. Compilation of all genes encoding two-component phosphotransfer signal transducers in the genome of *Escherichia coli*. *DNA Res.* **4,** 161–168 (1997).
14. Ota, I. M. & Varshavsky, A. A yeast protein similar to bacterial two-component regulators. *Science* **262,** 566–569 (1993).
15. Soncini, F. C. & Groisman, E. A. Two-component regulatory systems can interact to process multiple environmental signals. *J. Bacteriol.* **178,** 6796–6801 (1996).
16. Dziejman, M. & Mekalanos, J. J. in *Two-Component Signal Transduction* (eds Hock, J. A. & Silhavy, T. J.) 305–317 (ASM, Washington, DC, 1995).
17. Barrett, J. F. *et al.* Antibacterial agents that inhibit two-component signal transduction systems. *Proc. Natl Acad. Sci. USA* **95,** 5317–5322 (1998).
18. Nilges, M., Gronenborn, A. M., Brünger, A. T. & Clore, G. M. Determination of three-dimensional structures of proteins by simulated annealing with interproton distance restraints. Application to crambin, potato carboxypeptidase inhibitor and barley serine proteinase inhibitor 2. *Protein Eng.* **2,** 27–38 (1988).
19. Brünger, A. T. *X-PLOR Version 3.1: A system for X-ray Crystallography and NMR* (Yale Univ. Press, New Haven, 1992).
20. Kraulis, P. J. MOLSCRIPT: a program to produce both detailed and schematic plots of protein structures. *J. Appl. Crystallogr.* **24,** 946–950 (1991).
21. Merritt, E. A. & Murphy, M. E. P. Raster 3D Version 2.0—a program for photorealistic molecular graphics. *Acta Crystallogr. D* **50,** 869–873 (1994).
22. Holdgate, C. A. *et al.* The entropic penalty of ordered water accounts for weaker binding of the antibiotic novobiocin to a resistant mutant of DNA gyrase: a thermodynamic and crystallographic study. *Biochemistry* **36,** 9663–9673 (1997).
23. Orengo, C. A., Brown, N. P. & Taylor, W. R. Fast structure alignment for protein databank searching. *Proteins* **14,** 139–167 (1992).

Acknowledgements. We thank L. Kay for providing NMR pulse sequences, L. Pearl for the Hsp90-ATP coordinates before PDB release and discussions, and S. Bagby for comments on the manuscript. This work was supported by grants from JSPS (to T.T.) from CREST (to M.K.) from the NIH (to M. Inouye), and from HHMI (to M. Ikura). R.I. and D.L. acknowledge HFSP postdoctoral fellowships. M. Ikura is an HHMI International Research Scholar and MRCC Scientist.

Correspondence and requests for materials should be addressed to M. Ikura (e-mail: mikura@oci.utoronto.ca). Coordinates have been deposited in the Brookhaven Protein Data Bank.

Structure of the haemagglutinin-esterase-fusion glycoprotein of influenza C virus

Peter B. Rosenthal*†, Xiaodong Zhang*†, Frank Formanowski†‡, Wolfgang Fitz†§, Chi-Huey Wong§, Herbert Meier-Ewert‡, John J. Skehel‖ & Don C. Wiley¶

** Department of Molecular and Cellular Biology, Harvard University, and ¶ Howard Hughes Medical Institute, 7 Divinity Avenue, Cambridge, Massachusetts 02138, USA*
‡ Abteilung für Virologie, Technical University of Munich, Biedersteiner Strasse 29, 80802 Munich 40, Germany
§ Department of Chemistry, The Scripps Research Institute, 10666 North Torrey Pines Road, La Jolla, California 92037, USA
‖ National Institute for Medical Research, The Ridgeway, Mill Hill, London NW7 1AA, UK

The spike glycoproteins of the lipid-enveloped orthomyxoviruses and paramyxoviruses have three functions: to recognize the receptor on the cell surface, to mediate viral fusion with the cell membrane, and to destroy the receptor. In influenza C virus, a single glycoprotein, the haemagglutinin-esterase-fusion (HEF) protein, possesses all three functions (reviewed in ref. 1). In influenza A and B, the first two activities are mediated by haemagglutinin and the third by a second glycoprotein, neuraminidase. Here we report

† Present addresses: MRC Laboratory of Molecular Biology, Hills Road, Cambridge, England CB2 2QH, UK (P.B.R.); Molecular Structure and Function Laboratory, Imperial Cancer Research Fund, 44 Lincoln's Inn Fields, London, WC2A 3PX, UK (X.Z.); Cressier, Switzerland (F.F.). Quest International, Bussum, The Netherlands (W.F.).